

# Submerged Membrane Photo Reactor (SMPR) with Simultaneous Photo Degradation and TiO<sub>2</sub> Catalyst Recovery for Efficient Dyes Removal

Dessy Ariyanti <sup>\*,1</sup>

Filicia Wicaksana <sup>2</sup>

Wei Gao <sup>2</sup>

<sup>1</sup> Department of Chemical Engineering, Universitas Diponegoro, Semarang 50275, Indonesia

<sup>2</sup> Department of Chemical & Materials Engineering, The University of Auckland, Auckland 1142, New Zealand

\*e-mail: [dessy.ariyanti@che.undip.ac.id](mailto:dessy.ariyanti@che.undip.ac.id)

*Submitted* 18 May 2021

*Revised* 03 October 2021

*Accepted* 08 October 2021

---

**Abstract.** In this study, a polyvinylidene difluoride (PVDF) hollow fiber membrane module incorporated with TiO<sub>2</sub> was submerged into a photocatalytic reactor to create a hybrid photocatalysis with membrane separation process (a submerged membrane photoreactor, SMPR), for advanced dyes wastewater treatment. The SMPR performance was assessed by the degradation of single component Rhodamine B (RhB) and degradation of mixed dyes (RhB and Methyl orange (MO)) in a binary solution. Several operational parameters such as the amount of catalyst loading, permeate flux, and the effect of aeration were studied. Fouling tendency on the membrane was also investigated to determine the optimum operating conditions. The results show that the synergetic effect of the low catalyst loading and permeate flux creates the environment for optimum light penetration for high photocatalytic activity as the hybrid system with low catalyst loading (0.5 g/L) and 66 L/m<sup>2</sup>h of flux with aeration at 1.3 L/min has proven to increase the photocatalysis performance by 20% with additional catalyst recovery. In addition, applying the low catalyst loading and flux permeate with aeration brings minimal fouling problems.

**Keywords:** Dye degradation, Submerged membrane, Photocatalytic reactor, TiO<sub>2</sub> recovery

## INTRODUCTION

Industrial dyes and textile dyes wastewater has been a long-term environmental threat. During the manufacturing process, about 10–20% of total dye products are become waste and discharged as effluents into the water body. The common pollutants found in textile wastewater and other industrial processes are organic dyes (Ajmal, Majeed, Malik, Idriss, &

Nadeem, 2014; Saravanan, Gracia, & Stephen, 2017; Zangeneh, Zinatizadeh, Habibi, Akia, & Hasnain Isa, 2015).

To date, the most reliable method in terms of zero waste technology for organic wastewater treatment is photocatalysis using catalyst semiconductor metal oxide TiO<sub>2</sub>. Under UV light exposure, TiO<sub>2</sub> excited electrons for hydroxyl radicals (•OH) generation, which further assists organic compounds' decomposition and

mineralization (Li, Lin, & Huang, 2009). Almost all types of organic components can be degraded by this method, as the reactions involve hydroxyl radicals that are non-selective reactions (Yan, Li, & Zou, 2010). This process is also economically viable as compared with other technologies.

In a large-scale water treatment process, powder form TiO<sub>2</sub> is preferable to film or other forms as it has larger surface-active sites that are favourable for the degradation process. The fixation of catalysts and catalyst immobilization will reduce the amount of catalyst active sites, increase the mass transfer resistance, and increase the operation difficulty, as the photon penetration might not easily reach every single surface site for photonic activation. However, the use of powder TiO<sub>2</sub> in the aqueous system requires an additional step for catalysts recovery. This process is important to recover the photocatalyst particles as well as to avoid the contamination of TiO<sub>2</sub> in the treated water (Chong, Jin, Chow, & Saint, 2010; Mozia, 2010; Sillanpää, Ncibi, & Matilainen, 2018). Photocatalytic membrane reactors (PMRs) is a promising solution to this issue, as it enhances the efficacy of classical photo-reactors (PRs) and those of membrane processes with a combined effect of both technologies, thus cutting environmental impact and improving the cost-effectiveness of the system (Molinari, R., Argurio, & Palmisano, 2015; Vatanpour, Darrudi, & Sheydaei, 2020).

A PMR combines a photocatalyst and a membrane to produce chemical transformations and separation simultaneously. Among several types of PMR, a submerged membrane photoreactor (SMPR) has great potential to be applied in a large-scale wastewater treatment system. In

this configuration, the catalyst is suspended in an aqueous solution and the membrane module and permeate is sucked through a vacuum pump (Molinari, R. et al., 2015; Molinari, Raffaele, Lavorato, & Argurio, 2017). Most studies of SMPRs have generally been limited to treating a single component (Jiang, Zhang, & Choo, 2017; López Fernández, Coleman, & Le-Clech, 2014; Vatanpour, Karami, & Sheydaei, 2017; Zheng, Wang, Chen, Wang, & Cheng, 2015), but the natures of both membrane fouling and photocatalysis are complex and have a significant influence on the performance of the system (Zhang, Ding, Luo, Jaffrin, & Tang, 2016). One study of SMPR investigated the effect of light intensity and reactor configuration in the application for polluted river water (Meng et al., 2005). More studies need to be conducted to affirm the critical operational parameters that play a role in the simultaneous process, which might differ depending on the inlet characteristics, type of catalyst and the reactor configuration used in the process.

In this paper, the performance of SMPR for the degradation of single component RhB and degradation of mixed dyes (RhB and MO) in the binary solution were investigated along with the operational parameters such as catalyst loading, permeate flux, and aeration. Fouling tendency on the membrane was also studied to determine the optimum operating condition.

## **MATERIALS AND METHODS**

### **Materials**

The photocatalyst used in this study is TiO<sub>2</sub> anatase nano-powder size < 25 nm. Rhodamine B (RhB) and Methyl orange (MO) were used as representative dyes with purity >95% and 85%, respectively. All chemicals

---

were purchased from Sigma Aldrich Co. LCC and used without purification.

### Evaluation of Photocatalytic Activity

The photocatalytic activity experiment used as a control was assessed by observing the degradation of dyes under black light irradiation. Photocatalyst (0.5; 1.0 and 2.0 g/L) was mixed with dyes solution (2 L, five ppm). For the single solution, TiO<sub>2</sub> was added to 5 ppm of dye (RhB) solution, while in the binary solution, it consisted of 5 ppm RhB and 5 ppm MO and TiO<sub>2</sub>. The amount of catalyst loading was 0.5, 1.0, and 2.0 g/L. After stirring for 60 min in the dark to reach the adsorption equilibrium, the solution was illuminated with UV Blacklight (20W) for 180 min. The sample (3 mL) was withdrawn in 60 minutes and filtered using a PVDF syringe filter 0.2 µm before spectrophotometric reading. Dye's concentration was determined by absorbance value at 463 nm for MO and 553 nm for RhB with Perkin Elmer Instrument UV-Vis spectrophotometer.

### SMPR Configuration and Procedures

SMPR used in this experiment is

schematically illustrated in Figure 1. The system consisted of a cylindrical reactor with an inner diameter of 100 mm and height of 300 mm, immersed lamp (black light 20W) protected by quartz tube glass, an immersed membrane unit that placed 40 mm distance from the light source, a peristaltic pump (Cole-Parmer Masterflex 77201-60), a pressure transducer (Cole-Parmer C-P68075-02), and data logging system (Metermaster TC08). A magnetic stirrer was placed at the bottom of the reactor for mixing purposes. An additional aeration system (air bubbling system 1.3 L/min) was also placed inside the reactor to investigate the effect of aeration in photocatalysis and membrane filtration performance. The membranes (purchased from Hinada Water Treatment Tech. Co. Ltd, China) were hydrophilic polyvinylidene difluoride (PVDF) hollow fiber membranes with a pore size of 0.01-0.4 µm, inner radius 0.6 mm and outer radius of 1.2 mm. 20 pieces of hollow fiber membranes with the effective length 200 mm were then manually assembled into a loop (U shape) with epoxy glue to achieve the effective membrane area of 0.0048 m<sup>2</sup>.

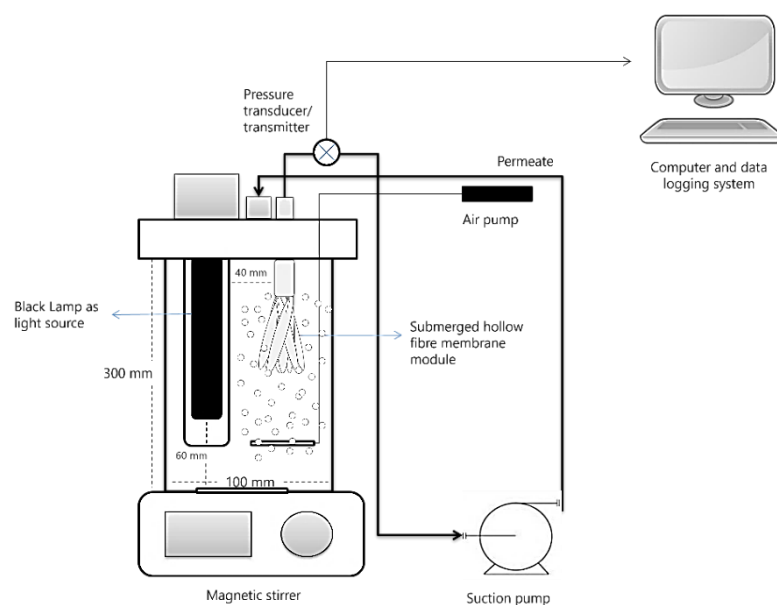


**Fig. 1:** Schematic Diagram of The Submerged Photocatalytic Membrane Reactor

The performance of the SMPR with the working volume of 2 L was evaluated at different catalyst loading (0.5; 1.0 and 2.0 g/L) and different permeate flux values (66; 110; 132 L/m<sup>2</sup>h) with and without aeration. The concentration and proportion of dyes in the single and binary solution were the same as those described in the previous section. The membrane filtration system was operated at constant flux for each run. Trans-membrane pressures (TMP) were auto-recorded at predetermined time intervals by a data logging system. The permeate flux was manually recorded every 30 min to ensure it was maintained at a constant level.

The feed solution (3 mL) sample was withdrawn in 60 minutes and filtered using PVDF syringe filter 0.2 μm before spectrophotometric reading. The concentration of aqueous dyes both in feed and permeate were determined with a UV-Vis spectrophotometer by observing the peak at wavelengths indicated in the previous section.

### Membrane Characterization

FTIR analysis of the before and after used membranes was conducted with Perkin Elmer FT-IR Spectroscopy Attenuated Total Reflectance (ATR). Meanwhile, the morphology of the membranes and the presence of TiO<sub>2</sub> nanoparticles were identified by Phenom ProX scanning electron microscope (SEM) with integrated Energy Dispersive Spectrometer (EDS).

### Performance Analysis

The first experiment was carried out to investigate the effect of feed solution on membrane performance. Three different feed solutions were prepared: (1) solution containing catalyst TiO<sub>2</sub> only, (2) solution

containing five ppm RhB without the catalyst, and (3) solution containing both compounds (0.5 g/L TiO<sub>2</sub> and five ppm RhB). The SMPR then was operated at the constant flux of 66 L/m<sup>2</sup>h for 200 min, while the TMP were automatically recorded. The feed solution and permeate samples were taken every 30 min to determine the % membrane rejection to the RhB compound.

The photocatalytic performance was analyzed by calculating the degradation efficiency and its kinetics constant. The degradation efficiency was calculated by using Eq. (1):

$$\text{Degradation efficiency} = \frac{C}{C_0} \quad (1)$$

where  $C_0$  is the initial concentration and  $C$  is the concentration of organic at a specific time.

The reaction kinetics can be calculated using the Langmuir-Hinshelwood model with notes that the concentration of adsorption in the dark condition is negligible. The reaction kinetics equation is expressed as in Eq. (2):

$$\ln \frac{C_0}{C_t} = kt \quad (2)$$

where  $C_0$  is initial concentration;  $C$  is the concentration of organic at the specific time;  $k$  is kinetics constant;  $t$  is time.

Meanwhile, the performance of the membrane was analyzed by monitoring the TMP over time and the dyes rejection of the membrane. TMP is the pressure gradient across the membrane. It is the effective pressure for forcing water through the membrane. TMP is calculated using Eq. (3):

$$TMP = P_{\text{feed}} - P_{\text{filtrate}} \quad (3)$$

where  $P_{\text{feed}}$  is the pressure measured during the soak/relaxation cycle (when no suction is applied to the membranes) and  $P_{\text{filtrate}}$  is the

---

pressure measured during the filtration cycle.

Rejection (R) in this system describes the removal of the total dye by the SMPR system, which includes degradation by photocatalyst, adsorption and retention by the membrane module. R is calculated as Eq. (4):

$$R = \left(1 - \frac{C_p}{C_f}\right) \times 100\% \quad (4)$$

where  $C_p$  and  $C_f$  are the concentrations of dyes in the permeate and initial feed solution, respectively. The concentration of dye was measured by UV Vis spectrophotometer.

## RESULTS AND DISCUSSION

### TiO<sub>2</sub> Photocatalytic Activity of RhB Degradation in SMPR System

The photocatalytic activity of TiO<sub>2</sub> for RhB degradation was evaluated in two different systems, (1) photocatalysis in the photoreactor without membrane and (2) simultaneous photocatalysis and catalyst recovery in the SMPR system at different amounts of catalyst loading. Figure 2 and Table 1 show that the photocatalytic activity of TiO<sub>2</sub> in the SMPR system is higher than in the photoreactor without the membrane. The peristaltic pressure that was applied for withdrawing clean water through the membrane and recirculating it back into the SMPR system might contribute to the additional hydrodynamic force in the solution, which increased the possibility of a photocatalytic reaction, thus increasing its kinetics constant and degradation efficiency.

In general, hydrodynamic force tends to reduce the kinetics rate of the reaction (Deutch & Felderhof, 1973; Du et al., 2017; Oppenheimer & Stone, 2017), however in the photocatalytic reaction, the reaction also depend on the opacity of the solution as it controls the light penetration to the

photocatalyst. The additional hydrodynamic force might reduce the opacity of the solution, thus leading to more light penetration into the photocatalyst and increasing the kinetics constant and degradation efficiency.

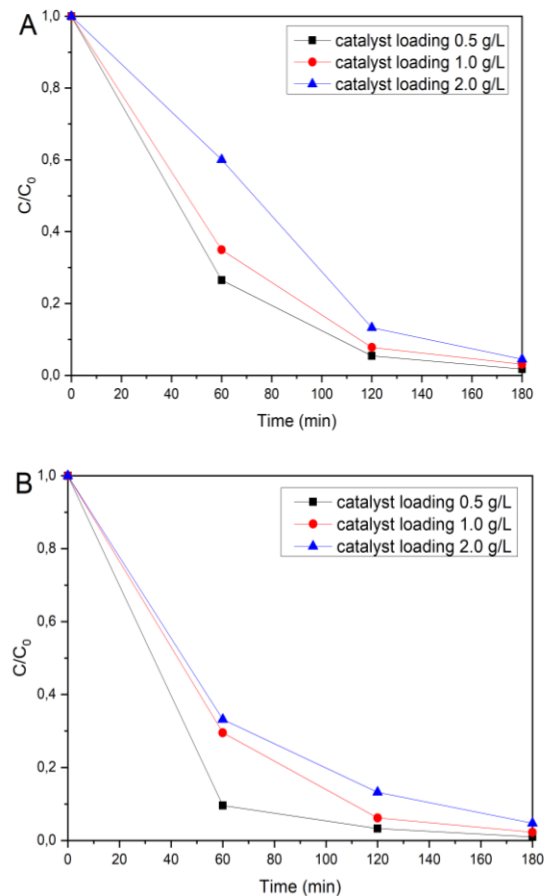


**Fig. 2:** Photodegradation profiles of RhB (A) Photocatalysis in Photo-Reactor and (B) Simultaneous Photocatalysis and Catalyst Recovery in SMPR System

The photocatalytic efficiency of TiO<sub>2</sub> depends on its concentration. As the amount of TiO<sub>2</sub> increases, the rate of oxidation rises. The amount of TiO<sub>2</sub> somehow controls the generation of free OH radicals. However, at some amount, high TiO<sub>2</sub> concentrations also decrease the penetration of UV radiation due to an increase in turbidity, which in turn affects the reaction rate negatively (Erdim, Soyer, Tasiyici, & Koyuncu, 2009).

**Table 1.** Kinetics Constant Data of Rhb Degradation at Different Catalyst Loading and Mode of The Process

Catalyst loading (g/L)	photocatalysis only at photo-reactor	
	k (/min)	R <sup>2</sup>
0.5	0.0230	0.9966
1.0	0.0198	0.9920
2.0	0.0165	0.9586
Catalyst loading (g/L)	simultaneous photocatalysis and catalyst recovery at SMPR	
	k (/min)	k (/min)
0.5	0.0275	0.0275
1.0	0.0216	0.0216
2.0	0.0170	0.0170

The level of opacity or turbidity is different depending on the type of dyes contained in wastewater. Thus, the amount of catalyst loaded into the system affects photon flux penetration (Nguyen et al., 2020). In this RhB degradation experiment, the optimum level was 0.5 g/L, and by using the same amount of catalyst loading in the SMPR system, the kinetics constant was increased almost 20%. Similar optimum catalyst loading was obtained by the previous researcher using different types of organic pollutants (Diclofenac) (Sarasidis, Plakas, Patsios, & Karabelas, 2014) and Acid Red 1 (Kertész, Cakl, & Jiránková, 2014).

### Effect of Feed Solution Characteristic

The first experiment was carried out to investigate the effect of feed solution on membrane performance. Figure 3 and Figure 4 illustrate the TMP profiles and % rejection of membrane at different feed solutions, respectively, after 3.5 hours operation time.

The slight variation of the TMP profiles of three different feed solutions containing TiO<sub>2</sub>, RhB and TiO<sub>2</sub>-RhB were observed. The

TMP of the RhB solution system was slightly fluctuating with a value mainly below 1.5 KPa.

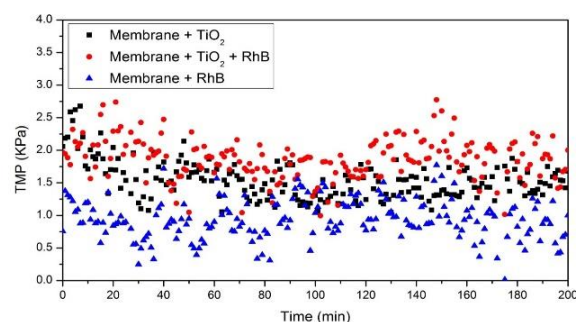


**Fig. 3:** TMP Profiles of The Membrane at Different Feed Solutions (Flux 66 L/m<sup>2</sup>h)

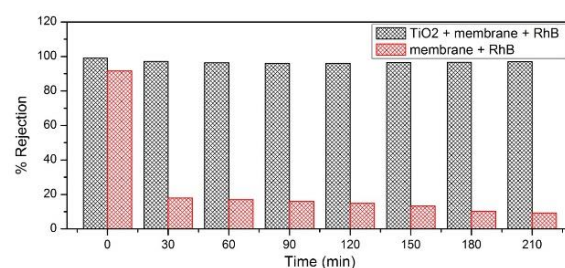


**Fig. 4:** Percent Rejection of RhB at Different Feed Solutions

Meanwhile, feed solutions containing TiO<sub>2</sub> were in the range of 1.5 to 2.5 KPa. Slightly higher TMP values of feed solution containing TiO<sub>2</sub> were due to some TiO<sub>2</sub> particles depositing on the membrane, thus increasing the TMP. Meanwhile, TMP values of the feed solution containing RhB are the lowest due to the size of RhB that can easily penetrate through the microfiltration membrane.

It is reflected by the membrane rejection of RhB (Figure 4). In operation without photocatalyst, the membrane passed through almost 90% of RhB. Meanwhile, the rejection of feed solution containing RhB and TiO<sub>2</sub> was higher up to 97%. It was due to the synergy between the degradation process by photocatalyst, adsorption and retention by the membrane module.

The data represented in Figure 3 can be analyzed further using the resistance in the series model. This model describes the relation between flux and TMP. The equation in this model is in-line with other equations used in air/water flow calculations, electric current flow, heat/mass transfer, etc., where the flux is related to the driving force (TMP) and inversely related to the resistances, as shown in the equation 5 (Yoon, 2015).

$$J = \frac{\Delta P_T}{\mu(R_m + R_c + R_f)} \quad (5)$$

where  $J$  is water flux (m/s);  $\Delta P_T$  is trans-membrane pressure (Pa or kg/m/s<sup>2</sup>);  $\mu$  is the viscosity of permeate (kg/m/s or cP,  $1.00 \times 10^{-3}$  for water at 20°C);  $R_m$  is membrane resistance (/m);  $R_m$  can be measured by filtering DI water through new membrane assuming  $R_c$  and  $R_f$  are zero. Total resistance can be measured from the operational data of feed solution filtration.  $R_f + R_c$  is calculated by subtracting  $R_m$  from the total resistance of the feed solution.  $R_f$  is irreversible fouling resistance (/m), and  $R_c$  is cake resistance (/m).  $R_f$  is often neglected and included in  $R_c$ , and  $R_f$  is typically insignificant compared to  $R_c$  and equally consistent in different filtration cycles (Yoon, 2015).

Figure 5 summarizes the comparison of membrane resistance ( $R_m$ ) and cake resistance ( $R_c$ ) of different feed solutions. The results emphasized that the cake resistance is dominant over membrane resistance.  $\text{TiO}_2$  contributes to the high cake resistance, as RhB was dissolved in the solution and penetrated through the membrane (Rejection membrane over RhB only 10%). In this case, the resistance value is used to determine the contribution of  $\text{TiO}_2$  and RhB on the membrane performance.

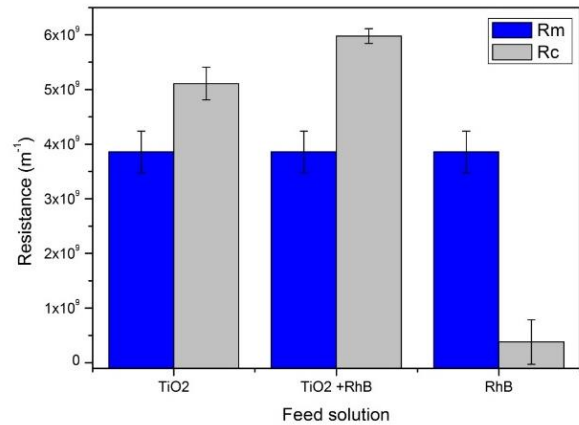


**Fig. 5:** Membrane Resistance ( $R_m$ ) and Cake Resistance ( $R_c$ ) of Different Feed Solutions

### Effect of Catalyst Loading

The effect of catalyst loading  $\text{TiO}_2$  on the membrane performance was also investigated. The membrane performance can be observed from the TMP profile and % rejection of organic pollutants during the process. Figure 6 illustrate the TMP profile of SMPR at different amount of catalyst loading. The TMP values of 1.0 and 2.0 g/L catalyst loading slowly increased from the initial value of around 2.25 KPa to 3.5 and 4.5 KPa, respectively.

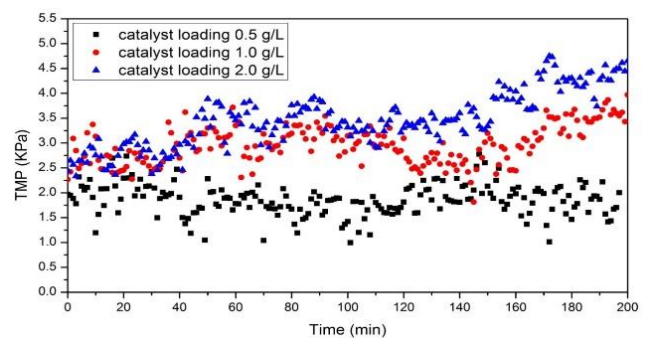


**Fig. 6:** TMP Profile of Simultaneous Mode, Process Running at Flux 66 L/m<sup>2</sup>h In Rhb Solution

Meanwhile, TMP values of the process with 0.5 g/L catalyst loading were relatively stable within the 2 KPa range. The higher concentration of catalyst  $\text{TiO}_2$  in the feed

solution is associated with a higher tendency of these particles to deposit on the membrane (so-called membrane fouling) (Nguyen et al., 2020; Yoon, 2015; Zhang et al., 2016). The deposited layer will act as an additional barrier that restricts the water passage through the membrane, increasing TMP.

**Table 2.** Rejection of RhB at Different Catalyst Loading

Time (min)	% Rejection		
	0.5 g/L	1.0 g/L	2.0 g/L
30	97.05	96.69	95.73
90	96.63	95.82	94.23
180	95.95	95.68	92.29

The rejection efficiency of the membrane toward RhB at different catalyst loading is displayed in Table 2. The process with the highest catalyst loading (2 g/L) has the lowest rejection, which is 92%. In comparison, the processes with catalyst loading 0.5 g/L and 1.0 g/L manage to have 96 and 95.6 % of rejection, respectively. A similar rejection percentage was found on the PSMR system, around 95% for diclofenac removal with catalyst loading 1 g/L (Nguyen et al., 2020).

The rejection of RhB is closely related to the degradation efficiency. Suppose the photocatalytic reaction is not fast enough to degrade RhB fully. In that case, there will be a higher chance for the non-degradable RhB to be absorbed onto the membrane surface and to penetrate through the membrane, contaminating the permeate water. By referring to Figure 2 and Table 1, the system's degradation efficiency and kinetics constant with 2 g/L catalyst loading are relatively lower than the other two values.

A lower kinetics constant indicates a higher RhB concentration left in the feed

solution. Hence, the higher chance of RhB adsorbed onto the membrane surface.

### Effect of Permeate Flux

Different flux values (66, 110, and 132 L/m<sup>2</sup>h) were applied to the system. TMP values and profiles at different permeate fluxes are shown in Figure 7. Results show slow increment along with the time. The increased TMP results from TiO<sub>2</sub> catalyst deposition on the membrane surface. The deposition is unavoidable due to the convection of feed solution towards the membrane surface during permeation (Yoon, 2015). As expected, higher flux values (110 and 132 L/m<sup>2</sup>h) produce higher TMP values (4.5 KPa and 5.75 KPa, respectively). While TMP values at the flux of 66 L/m<sup>2</sup>h range from 2 to 2.5 KPa.

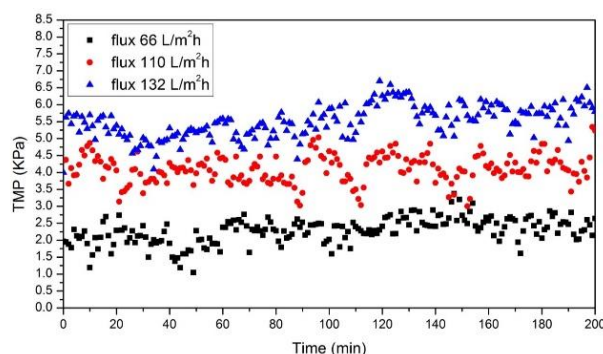


**Fig. 7:** TMP Profiles of Simultaneous Mode Process Running at Different Permeate Flux with 0.5 g/L Catalyst Loading

**Table 3.** Rejection of RhB at Different Permeate Flux

Time (min)	% Rejection		
	66 L/m <sup>2</sup> h	110 L/m <sup>2</sup> h	132 L/m <sup>2</sup> h
30	97.05	93.02	90.69
90	96.63	92.19	20.18
180	95.95	92.03	18.65

Table 3 displays the rejection of RhB at different permeate flux values. The highest

rejection is achieved at the lowest flux value. Meanwhile, an extremely low rejection (18%) is generated from the system with a high flux value (132 L/m<sup>2</sup>h).

High flux values were followed by relatively high vacuum pressure applied to the membrane. This high pressure drives high and fast TiO<sub>2</sub> deposition on the membrane surface. As a large amount of TiO<sub>2</sub> is deposited on the membrane surface, the concentration of TiO<sub>2</sub> in the feed solution that acts as a catalyst for the degradation process is reduced, thus leading to the low degradation efficiency and low kinetics constant.

The kinetics constant of flux value 110 and 132 L/m<sup>2</sup>h is 0.0247min<sup>-1</sup> (R<sup>2</sup> = 0.9503) and 0.006 min<sup>-1</sup> (R<sup>2</sup> = 0.9537) respectively. As stated in the previous section, the rejection of RhB is closely related to degradation efficiency. Due to high RhB concentration remains in the feed solution (35% from the initial concentration), and at the same time, adsorption of RhB into the membrane occurred. Thus water that withdraws from the system will carry a high concentration of RhB.

### Effect of Aeration

The effect of aeration on the membrane performance was evaluated by monitoring the TMP profiles of the SMPR system without and with aeration at flux 66 L/m<sup>2</sup>h using 2.0 g/L catalyst loading. There was a noticeable difference in the TMP profile, as displayed in Figure 8. The TMP value of SMPR without aeration was higher after 60 min of operation, and it continued increasing from 2.5 KPa to 4.5 KPa.

Meanwhile, the TMP profile of the system with aeration is relatively stable in the range value of 2 to 3 KPa. Aeration can minimize the fouling by creating shear, which improves the mixing of particles in the

solution and limits their attachment to the membrane surface. In addition, as the air bubbles are generated, it scrubs the membrane surface and disengage the cake layer on the membrane surface. Those processes will increase membrane water flux, or if the system operated at constant flux, it could reduce the TMP value. (Ong, Lau, Goh, Ng, & Ismail, 2014; Zhang et al., 2016). Aeration can also increase photocatalytic activity, as the aeration provides additional oxygen sources that can be converted into reactive oxygen and hydroxyl radical favorable for the degradation process (Ong et al., 2014; Vatanpour et al., 2020; Zhang et al., 2016). The kinetics constant of SMPR without aeration is recorded about 0.017 min<sup>-1</sup> (R<sup>2</sup> = 0.9986), while with aeration is 0.0241 min<sup>-1</sup> (R<sup>2</sup> = 0.9503), increase about 42%.

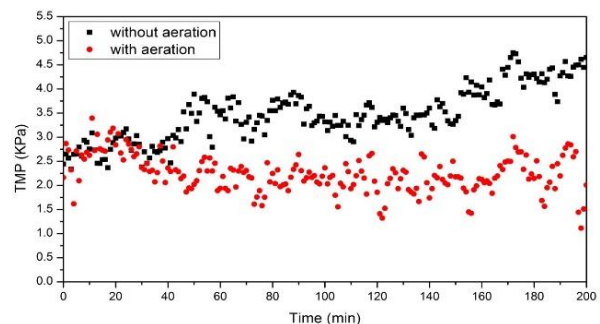


**Fig. 8:** TMP Profiles of Simultaneous Mode Process Running at Flux 66 L/m<sup>2</sup>h with 2.0 g/L Catalyst Loading with and without Aeration in Rhb Solution

**Table 4.** Rejection of Rhb at System with and without Aeration

Time (min)	% Rejection	
	without aeration	with aeration
30	98.20	97.49
90	93.38	96.58
180	92.28	96.03

The increment of kinetics constant will also increase the % rejection as the rejection

of RhB is closely related to the degradation efficiency. Table 4 display the comparison of rejection of RhB at the system with and without aeration.

### Fouling Observation

The main technical drawback of the SMPR system to be applied in the wastewater treatment field is membrane fouling. Membrane fouling is a process whereby a solution or a particle is deposited on a membrane surface or in membrane pores. This phenomenon could eventually decrease the performance and efficiency of the filtration process and increase the operating cost. In SMPR, both pollutants and photocatalysts may contribute to membrane fouling. The phenomena can be observed from the operating condition profiles such as permeate flux and TMP.

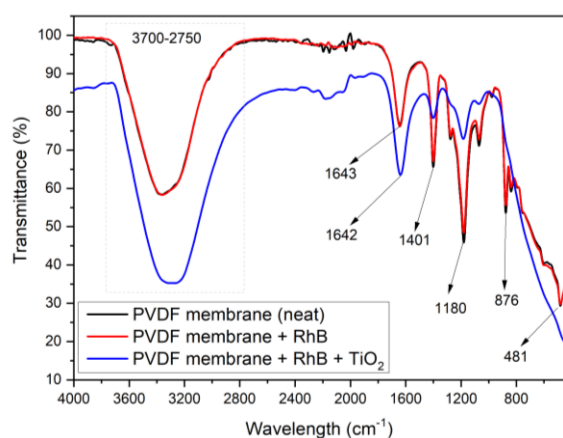


**Fig. 9:** FT-IR Analysis of PVDF Membrane before and after Used

FTIR analysis result of the PVDF membrane before and after being used was displayed in Figure 9. The neat membrane can be easily identified as PVDF as stretching frequencies were observed in the region 2750-3700 cm<sup>-1</sup>, and a strong band at 1401 cm<sup>-1</sup>; indicates the presence of CH<sub>2</sub> group (Stuart, 2004). The weak band at 1074 cm<sup>-1</sup>

and a strong band at 876 cm<sup>-1</sup> are assigned to C-C stretching. In addition, a strong band at 1180 cm<sup>-1</sup> and a weak band at 481 cm<sup>-1</sup> represent CF<sub>2</sub>.

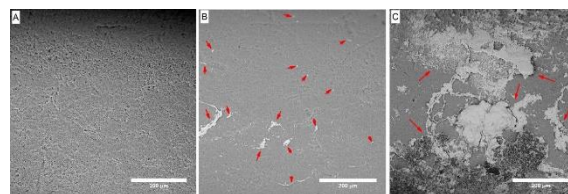


**Fig. 10:** Surface SEM Images of (A) Neat Membrane, (B) Membrane after Used at Catalyst Loading 0.5 g/L and (C) Membrane after Used at Catalyst Loading 2.0 g/L

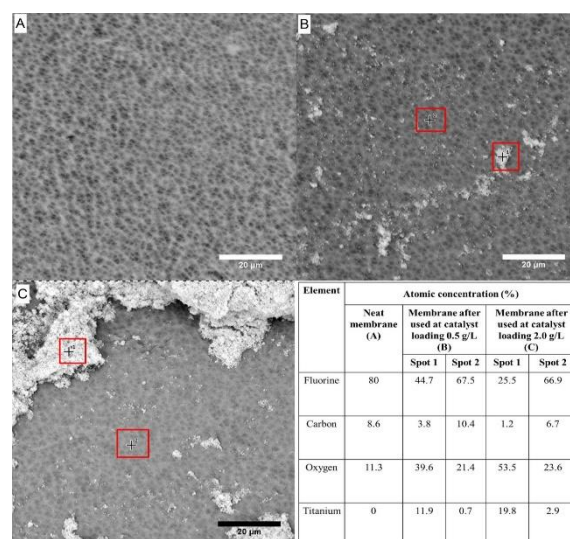


**Fig. 11:** Surface SEM Images of (A) Neat Membrane, (B) Membrane after Used at Catalyst Loading 0.5 g/L, (C) Membrane after Used at Catalyst Loading 2.0 g/L (at Higher Magnification) and EDS Analysis of Spots on The Samples

Meanwhile, the after used membrane shows no band below 1000 cm<sup>-1</sup> indicates the presence of TiO<sub>2</sub> covering the surface of the membrane. Fouling also can be observed by comparing the SEM image of the membrane before and after the simultaneous photodegradation and catalyst recovery process. Figure 10 shows the SEM images of

membrane surfaces before (A) and after the process (B-C).

The small  $\text{TiO}_2$  nanoparticles were randomly agglomerated at some spot on the membrane surface after being used at catalyst loading 0.5 g/L (Figure 11B). The fouling was more severe at higher catalyst loading (2.0 g/L), as shown in Figure 11C.  $\text{TiO}_2$  nanoparticles were deposited and formed a thick cake layer on the membrane surface.

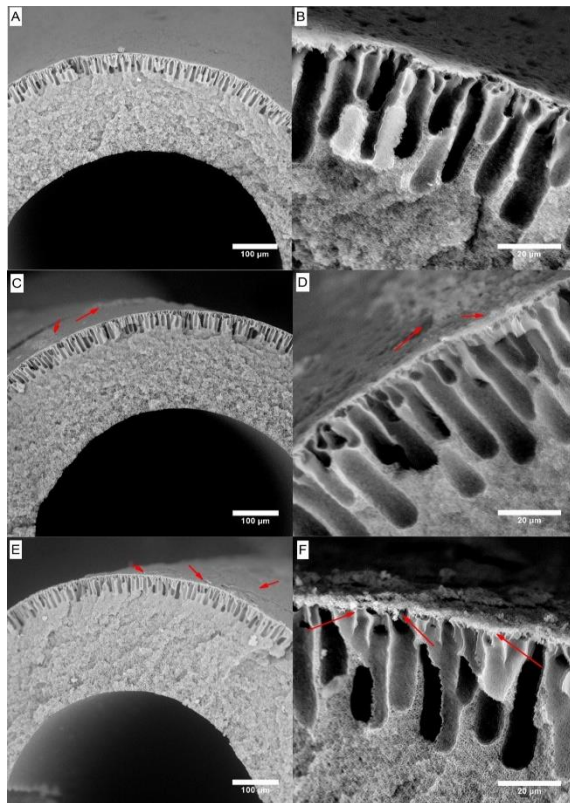


**Fig. 12:** Cross-section SEM Images of (A, B) Neat Membrane, (C, D) Membrane after Used at Catalyst Loading 0.5 g/L, and (E, F) Membrane after Used at Catalyst Loading 2.0 g/L

EDS analysis resumed in Figure 11 shows the rough estimation of the  $\text{TiO}_2$  percentage deposited on the membrane surface. The higher the catalyst loading added in the process, the higher the  $\text{TiO}_2$  percentage deposited on the membrane

surface. The highest titanium atomic percentage is 19.8% deposited on the membrane surface from the SMPR system that used high catalyst loading (2.0 g/L). Meanwhile, RhB was absorbed onto the resulting colored membrane as it is dissolved easily in water. No RhB was detected in the cake layer.

Figure 12 shows the cross-section SEM images of the membrane before (A-B) and after the process (C-F). In this case, it was observed that the thickness of the  $\text{TiO}_2$  cake layer deposited on the membrane surface depended on the catalyst loading used in the process.

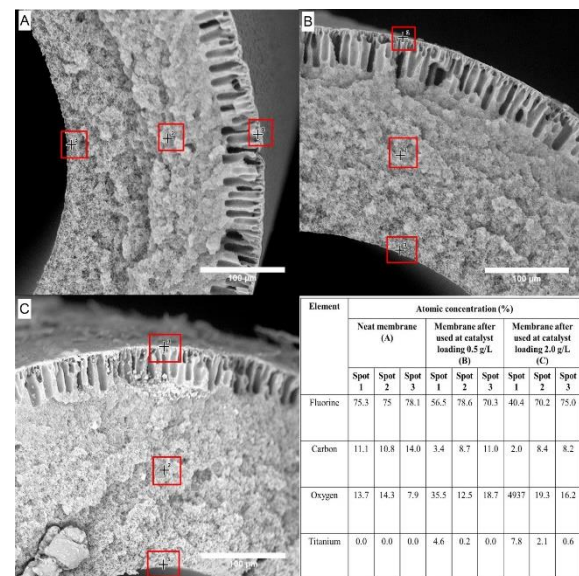


**Fig. 13:** Cross-section SEM Images of (A) Neat Membrane, (B) Membrane after Used at Catalyst Loading 0.5 g/L, (C) Membrane after Used at Catalyst Loading 2.0 g/L and EDS Analysis of Spots on The Samples

High catalyst loading (2 g/L) will form 3-4 microns layer during 3-4 hours of the continuous process, which is unfavorable for the performance of SMPR. Meanwhile, by employing low catalyst loading (0.5 g/L), a thin cake layer was formed on the membrane

surface (0-2 micron), as shown in Figure 12D.

EDS analysis resumed in Figure 13 shows the rough estimation of the TiO<sub>2</sub> percentage penetrates through the membrane from the surface to the inner side of the hollow fiber. The higher the catalyst loading added in the process, the higher the TiO<sub>2</sub> percentage deposited on the membrane surface. The atomic percentage of titanium in the membrane surface used in the system with 0.5 g/L and 2.0 g/L is 4.6 and 7.8 %, respectively. In addition, at high catalyst loading, TiO<sub>2</sub> was able to penetrate through the inner side of the membrane as much as 0.6%, while at low catalyst loading, the penetration was only up to the center of the membrane with 0.2 % of titanium detected. However, this amount can be considered insignificant. The penetration of TiO<sub>2</sub> nanoparticles was likely due to the membrane pore size distribution (0.01-0.4 μm), which is relatively wide, and the size of TiO<sub>2</sub> nanoparticles used as catalyst is around 21 nm. Penetration of TiO<sub>2</sub> nanoparticles is not favorable. They will become a contaminant in the clean water, withdraw from the system and reduce the amount of TiO<sub>2</sub> nanoparticles assigned as a catalyst for photocatalysis purposes in the system.

### Application of TiO<sub>2</sub> SMPR for Mixed Dyes Degradation

The application of SMPR for simultaneous photodegradation and catalyst recovery for mixed dyes solution (RhB and MO) was also studied by evaluating the photocatalytic activity and membrane performance at different catalyst loading (Table 5). In the mixed dyes system, one of the compounds degrades faster than the other. According to earlier research, the MO degradation kinetics constant is lower than RhB (Ariyanti, Maillot, & Gao, 2018).

Although the hydroxyl radical reaction is considered non-selective and will practically react with almost all the organic components (Yan et al., 2010), the variation of dyes chemical structures will still affect the reaction kinetics (Mozia, 2010). MO has an azo group (-N=N-) with the sulfonic group on the other side. These forms of bonding are related to high dissociation energy and less reactivity (Horikoshi, Saitou, Hidaka, & Serpone, 2003; Luan & Xu, 2013) contrasted with RhB functional groups. Low catalyst loading (0.5 g/L) is still favorable for the photocatalytic process in the SMPR system. It gives an optimum condition to UV light to penetrate and activate the TiO<sub>2</sub> surface, which further generates hydroxyl radical for degradation reaction.

**Table 5.** Kinetics Constant Data of Mixed Dyes Degradation at Different Catalyst Loading

Catalyst loading (g/L)	RhB		MO	
	k (/min)	R <sup>2</sup>	k (/min)	R <sup>2</sup>
0.5	0.0084	0.9749	0.0033	0.9999
1.0	0.0050	0.9864	0.0032	0.9919
2.0	0.0035	0.9327	0.0032	0.9625

In comparison with SMPR performance with single component feed solution, the photocatalytic activity of TiO<sub>2</sub> to degrade RhB in mixed dyes solution (RhB + MO) decreased down to 69%. The main reason is the amount of hydroxyl radical to react with RhB become lower in the presence of MO as a reaction competitor. The same amount of hydroxyl radical produced from the exact amount of catalyst loading is used to degrade RhB and MO simultaneously. Thus, the rate of reaction of RhB in SMPR with mixed dyes solution is slower than in SMPR with a single component (Ariyanti et al., 2018).

Meanwhile, the comparison of filtration performance of SMPR with single dye and mixed dyes solution can be seen in Figure 15. The TMP profiles of both solutions were relatively similar and scattering in the range of 1.0 to 3.0 KPa. Slightly higher TMP values were observed along with the time due to some  $\text{TiO}_2$  particles depositing on the membrane, thus increasing the transmembrane pressure due to membrane fouling. Different TMP profiles were hardly found in SMPR with single dye and mixed dyes solution. The explanation refers to the discussion section in the previous section, which stated that  $\text{TiO}_2$  is the main component contributing to the high cake resistance. This result also affirms that the primary component that drives the membrane filtration performance in this SMPR system is the  $\text{TiO}_2$ .

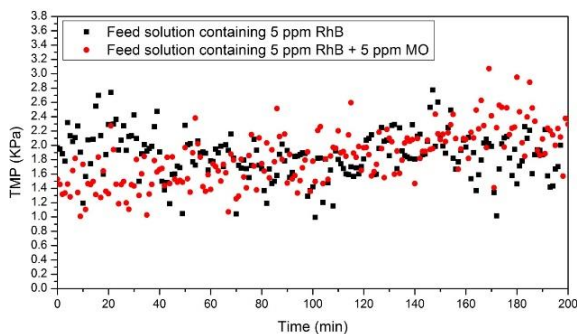


**Fig. 15:** Comparison of TMP Profiles of Feed Solution Containing Single and Binary Components With Permeate Flux  $66 \text{ L/m}^2\text{h}$  And Catalyst Loading  $0.5 \text{ g/L}$

**Table 6.** % Rejection of RhB in SMPR with Feed Solution Containing Single and Binary Components

Time (min)	% Rejection	
	single component	binary component
30	97.05	96.55
90	96.63	82.05
180	95.95	72.78

Table 6 compares RhB rejection in SMPR with feed solution containing single and binary components. As mentioned previously, the % rejection of RhB is related to the degradation efficiency.

The low degradation efficiency of RhB in SMPR with mixed dyes lead to a low % rejection (72.78%). Compared to SMPR in a single component, it decreases by around 23%. In the mixed dyes system, the photocatalytic activity of dyes degradation is relatively low, and it drives the overall membrane performance, especially the percentage of rejection.

## CONCLUSIONS

The performance of SMPR with simultaneous photodegradation and  $\text{TiO}_2$  catalyst recovery for efficient dyes removal were investigated. SMPR was proven to increase the photocatalytic activity up to 20%, with the additional advantage of recovering the catalyst. In the system with dyes as organic pollutant and  $\text{TiO}_2$  as the catalyst,  $\text{TiO}_2$  stand as the main contributor to the high resistance that influences the performance of the filtration process by the membrane. In the SMPR system that operated for degradation of single dye and mixed dyes, several parameters such as catalyst loading, permeate flux and aeration were found to affect the photocatalytic activity and filtration efficiency. Low catalyst loading ( $0.5 \text{ g/L}$ ) and low flux permeate ( $66 \text{ L/m}^2\text{h}$ ) are proven for optimum performance, as they can increase the light penetration for high photocatalytic activity and minimize the tendency of membrane fouling. Aeration can also be used to minimize the fouling problem based on the generation of the circulation flow and provide additional oxygen sources for photocatalytic reaction. The photocatalytic

activity drives the overall membrane performance, especially the rejection percentage.

#### ACKNOWLEDGEMENT

The authors thank the Advanced Materials Group of the Department of Chemical and Materials Engineering, the University of Auckland, for their assistance.

#### REFERENCES

1. Ajmal, A., Majeed, I., Malik, R. N., Idriss, H., & Nadeem, M. A. (2014). Principles and mechanisms of photocatalytic dye degradation on TiO<sub>2</sub> based photocatalysts: A comparative overview. *RSC Advances*, 4(70), 37003-37026. doi:10.1039/C4RA06658H
2. Ariyanti, D., Maillot, M., & Gao, W. (2018). Photo-assisted degradation of dyes in a binary system using TiO<sub>2</sub> under simulated solar radiation doi://doi.org/10.1016/j.jece.2017.12.031
3. Chong, M. N., Jin, B., Chow, C. W. K., & Saint, C. (2010). Recent developments in photocatalytic water treatment technology: A review. *Water Research*, 44(10), 2997-3027. doi:10.1016/j.watres.2010.02.039
4. Deutch, J. M., & Felderhof, B. U. (1973). Hydrodynamic effect in diffusion-controlled reaction. *The Journal of Chemical Physics*, 59(4), 1669-1671. doi:10.1063/1.1680247
5. Du, X., Qu, F., Liang, H., Li, K., Bai, L., & Li, G. (2017). Control of submerged hollow fiber membrane fouling caused by fine particles in photocatalytic membrane reactors using bubbly flow: Shear stress and particle forces analysis doi://doi.org/10.1016/j.seppur.2016.08.011
6. Erdim, E., Soyer, E., Tasiyici, S., & Koyuncu, I. (2009). Hybrid photocatalysis / submerged microfiltration membrane system for drinking water treatment. *Desalination and Water Treatment*, 9(1-3), 165-174. doi:10.5004/dwt.2009.767
7. Horikoshi, S., Saitou, A., Hidaka, H., & Serpone, N. (2003). Environmental remediation by an integrated microwave/UV illumination method. V. thermal and nonthermal effects of microwave radiation on the photocatalyst and on the photodegradation of rhodamine-B under UV/vis radiation. *Environmental Science & Technology*, 37(24), 5813-5822. doi:10.1021/es030326i
8. Jiang, L., Zhang, X., & Choo, K. (2017). Submerged microfiltration-catalysis hybrid reactor treatment: Photocatalytic inactivation of bacteria in secondary wastewater effluent doi://doi.org/10.1016/j.seppur.2017.01.018
9. Kertész, S., Cakl, J., & Jiráňková, H. (2014). Submerged hollow fiber microfiltration as a part of hybrid photocatalytic process for dye wastewater treatment. *Desalination*, 343, 106-112. doi:10.1016/j.desal.2013.11.013
10. Li, M., Lin, H., & Huang, C. (2009). Nanotechnostructured catalysts TiO<sub>2</sub> nanoparticles for water purification. (pp. 43-92) American Society of Civil Engineers. doi:10.1061/9780784410301.ch03 Retrieved from <http://dx.doi.org/10.1061/9780784410301.ch03>
11. López Fernández, R., Coleman, H. M., & Le-Clech, P. (2014). Impact of operating conditions on the removal of endocrine disrupting chemicals by membrane photocatalytic reactor. *Environmental*

- 
- Technology (United Kingdom)*, 35(16), 2068-2074.  
doi:10.1080/09593330.2014.892539
12. Luan, J., & Xu, Y. (2013). *Photophysical property and photocatalytic activity of new Gd<sub>2</sub>InSbO<sub>7</sub> and Gd<sub>2</sub>FeSbO<sub>7</sub> compounds under visible light irradiation* doi:10.3390/ijms14010999
  13. Meng, Y., Huang, X., Yang, Q., Qian, Y., Kubota, N., & Fukunaga, S. (2005). Treatment of polluted river water with a photocatalytic slurry reactor using low-pressure mercury lamps coupled with a membrane. *Desalination*, 181(1), 121-133. doi:10.1016/j.desal.2005.02.015
  14. Molinari, R., Argurio, P., & Palmisano, L. (2015). 7 - photocatalytic membrane reactors for water treatment. In A. Basile, & A. C. K. Rastogi (Eds.), *Advances in membrane technologies for water treatment* (pp. 205-238). Oxford: Woodhead Publishing. doi://dx.doi.org.ezproxy.auckland.ac.nz/10.1016/B978-1-78242-121-4.00007-1 Retrieved from <http://www.sciencedirect.com.ezproxy.auckland.ac.nz/science/article/pii/B9781782421214000071>
  15. Molinari, R., Lavorato, C., & Argurio, P. (2017). Recent progress of photocatalytic membrane reactors in water treatment and in synthesis of organic compounds. A review. *Catalysis Today*, 281, Part 1, 144-164. doi://dx.doi.org/10.1016/j.cattod.2016.06.047
  16. Mozia, S. (2010). Photocatalytic membrane reactors (PMRs) in water and wastewater treatment. A review. *Separation and Purification Technology*, 73(2), 71-91. doi://dx.doi.org/10.1016/j.seppur.2010.03.021
  17. Nguyen, V., Tran, Q. B., Nguyen, X. C., Hai, L. T., Ho, T. T. T., Shokouhimehr, M., . . . Van Le, Q. (2020). Submerged photocatalytic membrane reactor with suspended and immobilized N-doped TiO<sub>2</sub> under visible irradiation for diclofenac removal from wastewater. *Process Safety and Environmental Protection*, 142, 229-237. doi: <https://doi.org/10.1016/j.psep.2020.05.041>
  18. Ong, C. S., Lau, W. J., Goh, P. S., Ng, B. C., & Ismail, A. F. (2014). Investigation of submerged membrane photocatalytic reactor (sMPR) operating parameters during oily wastewater treatment process. *Desalination*, 353, 48-56. doi:10.1016/j.desal.2014.09.008
  19. Oppenheimer, N., & Stone, H. A. (2017). Effect of hydrodynamic interactions on reaction rates in membranes. *Biophysical Journal*, 113(2), 440-447. doi:10.1016/j.bpj.2017.06.013
  20. Sarasidis, V. C., Plakas, K. V., Patsios, S. I., & Karabelas, A. J. (2014). Investigation of diclofenac degradation in a continuous photocatalytic membrane reactor. influence of operating parameters. *Chemical Engineering Journal*, 239, 299-311. doi:10.1016/j.cej.2013.11.026
  21. Saravanan, R., Gracia, F., & Stephen, A. (2017). Basic principles, mechanism, and challenges of photocatalysis. In M. M. Khan, D. Pradhan & Y. Sohn (Eds.), *Nanocomposites for visible light-induced photocatalysis* (pp. 19-40). Cham: Springer International Publishing. doi:10.1007/978-3-319-62446-4\_2 Retrieved from [https://doi.org/10.1007/978-3-319-62446-4\\_2](https://doi.org/10.1007/978-3-319-62446-4_2)
  22. Sillanpää, M., Ncibi, M. C., & Matilainen, A. (2018). Advanced oxidation processes for the removal of natural organic matter from drinking water sources: A comprehensive review. *Journal of Environmental Management*, 208, 56-76.
-

- doi://doi.org/10.1016/j.jenvman.2017.12.009
23. Stuart, B. H. (2004). *Infrared spectroscopy: Fundamentals and applications*. Hoboken: John Wiley & Sons, Incorporated. Retrieved from <http://ebookcentral.proquest.com/lib/auckland/detail.action?docID=194354>
24. Vatanpour, V., Darrudi, N., & Sheydaei, M. (2020). A comprehensive investigation of effective parameters in continuous submerged photocatalytic membrane reactors by RSM. *Chemical Engineering and Processing - Process Intensification*, 157, 108144. doi:<https://doi.org/10.1016/j.cep.2020.108144>
25. Vatanpour, V., Karami, A., & Sheydaei, M. (2017). Central composite design optimization of rhodamine B degradation using TiO<sub>2</sub> nanoparticles/UV/PVDF process in continuous submerged membrane photoreactor doi:<https://doi.org/10.1016/j.cep.2017.02.015>
26. Yan, S. C., Li, Z. S., & Zou, Z. G. (2010). Photodegradation of rhodamine B and methyl orange over boron-doped g-C<sub>3</sub>N<sub>4</sub> under visible light irradiation. *Langmuir*, 26(6), 3894-3901. doi:[10.1021/la904023j](https://doi.org/10.1021/la904023j)
27. Yoon, S. H. (2015). *Membrane bioreactor processes: Principles and applications* CRC Press. Retrieved from <https://www.crcpress.com/Membrane-Bioreactor-Processes-Principles-and-Applications/Yoon/p/book/9781482255836>
28. Zangeneh, H., Zinatizadeh, A. A. L., Habibi, M., Akia, M., & Hasnain Isa, M. (2015). Photocatalytic oxidation of organic dyes and pollutants in wastewater using different modified titanium dioxides: A comparative review. *Journal of Industrial and Engineering Chemistry*, 26, 1-36. doi:[10.1016/j.jiec.2014.10.043](https://doi.org/10.1016/j.jiec.2014.10.043)
29. Zhang, W., Ding, L., Luo, J., Jaffrin, M. Y., & Tang, B. (2016). Membrane fouling in photocatalytic membrane reactors (PMRs) for water and wastewater treatment: A critical review doi:<https://doi.org/10.1016/j.cej.2016.05.071>
30. Zheng, X., Wang, Q., Chen, L., Wang, J., & Cheng, R. (2015). Photocatalytic membrane reactor (PMR) for virus removal in water: Performance and mechanisms. *Chemical Engineering Journal*, 277, 124-129. doi:[10.1016/j.cej.2015.04.117](https://doi.org/10.1016/j.cej.2015.04.117)
-